ESTIMATING SOIL SALINITY USING REMOTE SENSING DATA

Luis Garcia, Ahmed Eldeiry and Ayman Elhaddad
Associate Professor and Ph.D. Candidates
Civil Engineering Department
Colorado State University
Fort Collins, CO 80523
Voice: 970-491-5144 FAX: 970-491-7626
E-mail:garcia@engr.colostate.edu

INTRODUCTION

Soil salinity is a severe environmental hazard (Hillel 2000) that impacts the growth of many crops. Human-induced salinization is the result of salt stored in the soil profile being mobilized by extra water provided by human activities such as irrigation (Szabolcs 1989). Salinization problems continue to spread around the world at a rate of up to 2 million hectares a year, offsetting a good portion of the increased productivity achieved by expanding irrigation (Postel 1999). Since the irrigated acreage in Colorado is fairly stable, any increase in soil salinity will have a direct impact on the agricultural production of the state.

Remotely sensed data has great potential for monitoring dynamic processes, including salinization. Remote sensing of surface features using aerial photography, videography, infrared thermometry, and multispectral scanners has been used intensively to identify and map salt-affected areas (Robbins and Wiegand 1990). Metternicht and Zinck (1997) provided an approach for mapping salt- and sodium-affected surfaces by combining digital image classification with field observation of soil degradation features and laboratory determinations in the semiarid valleys of Cochabamba, Bolivia. Multispectral data acquired from platforms such as Landsat, SPOT, and the Indian Remote Sensing (IRS) series of satellites have been found to be useful in detecting, mapping and monitoring salt-affected soils (Dwivedi and Rao 1992).

Band ratios of visible to near-infrared and between infrared bands have proven to be better for identifying salts in soils and salt-stressed crops than individual bands (Craig et al., 1998 and Hick and Russell, 1990). Wiegand et al. (1994) carried out a procedure to assess the extent and severity of soil salinity in fields in terms of economic impact on crop production and effectiveness of reclamation efforts. Their results illustrate practical ways to combine image analysis

capability, spectral observations, and ground truth to map and quantify the severity of soil salinity and its effects on crops.

Ghabour and Daels (1993) concluded that detection of soil degradation by conventional means of soil surveying requires a great deal of time, but remote sensing data and techniques offer the possibility for mapping and monitoring these processes more efficiently and economically. However, to assess the accuracy of the ability of satellite images to map and monitor salinity, it is necessary to compare them with field measurements of salinity. Our research uses remote sensing techniques for the purpose of determining the spatial and temporal (if multiple images are used from different dates) extent and magnitude of salt-affected areas. We have focused our initial studies in an area around La Junta, in the Arkansas Valley of Colorado. We have used extensive field data to validate the accuracy of the remote sensing techniques.

METHODOLOGY

The approach presented in this paper involves integrating remote sensing data, Geographic Information System (GIS), and spatial analysis to predict soil salinity. First, soil salinity data was collected in the field. The locations of the field samples were recorded on a Global Positioning System (GPS) unit, and a GIS map was generated. The collected soil salinity data was tied to the corresponding points on a georeferenced Ikonos satellite image. The soil salinity data are tested against the blue, green, red, and infrared bands of the satellite image as well as the normalized difference vegetation index (NDVI) and the infrared band divided by the red band (IR/R). Stepwise regression is used to determine the combination of bands that best relate to soil salinity. Ordinary least squares (OLS), spatial autoregressive (SAR), and spatial lag (SLAG) models are used as regression models to correlate the variables. The weighted average of the resultant matrix from the soil salinity data and the corresponding value from the satellite imagery is determined.

We are also testing a second approach in which we assume that the crop condition is the main indicator of the presence and severity of saline soils. Elevated levels of soil salinity will affect the growth of most crops as well as their appearance. This can be detected remotely using satellite images. By enhancing the image, we can separate the crop condition into several classes. Using spatially referenced ground data collected at the study area, we can relate each class in the satellite image to a level of soil salinity. We can use these classes to create a signature file to classify other areas planted with the same crop.

As part of this project we have collected soil samples from over 100 locations, with each sample being comprised of four depths (1, 2, 3, and 4 feet). These samples were analyzed using the HACH SIW Salinity Appraisal, and a composite EC_e (the average of four sub samples at each 1 foot depth) was calculated for each sample. The calculated EC_e values were compared to the EM-38 readings

that were taken at each sample point. After multiple iterations it was decided that a linear regression between the EM-38 vertical reading and the EC_e provided the best match (Figure 1). From these data we developed the following regression model that converts EM-38 vertical readings into dS/m values:

F = (SStemp-25)/10
where: SStemp = temperature of soil sample measured in deg C
A = 1-0.203462 F + 0.038223 (F^2) - 0.005554 (F^3)
SSTc = A * SStemp (where: SSTc = temperature correction factor)
EM_{Vc} = EM_V * SSTc (where: EM_{Vc} = Temperature corrected EM-38 vertical reading)
EC_e = 0.0877 * EM_{Vc} + 1.8303

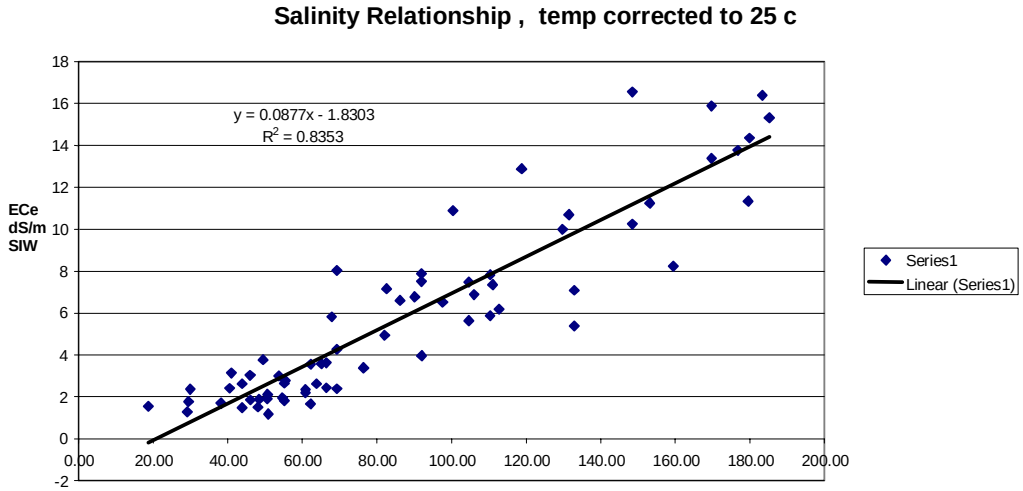

Figure 1. Regression equation relating EM_v and EC_e.

If equations with better correlations are developed to relate EM-38 readings to EC_e, the work presented here can be updated to reflect these new equations. However the methodology and approach will remain the same.

Analysis and Results

The criteria for selecting the best model are that it should have the smallest Akaike Information Corrected Criteria (AICC), a small standard error, a p-value of each selected variable less than 0.05, and a p-value of Moran's I of residuals larger than 0.05. For the combination of variables shown in Table 1, the OLS model using a combination of the blue band, infrared band, NDVI, and IR/R created the most accurate map of soil salinity for the given combination of variables. The SAR model was rejected because the p-value of the blue band was 0.3739. The SLAG model was also rejected because the p-values for both blue and infrared bands were larger than 0.05. For the OLS model, the p-value of Lagrange was 0 and the p-value of Moran's I was greater than 0.05. The equation to predict soil salinity based on the results of the OLS model is:

OLS predicted soil salinity = 8.5537 + 0.0099 * blue band – 0.87 * infrared band – 5.1164 * NDVI + 0.8918 * IR/R.

Table 1. The output variable results of OLS, SAR, and SLAG models using blue, infrared, NDVI, and IR/R.

Variable		OLS	SAR	SLAG
	R^2	0.524	0.2484	0.2401
	Residual Standard error	1.5598	1.3299	1.3544
Intercept	Coefficient	8.5537	7.6347	3.3836
	p-value	0	0.0106	0.0276
	Standard Error	1.7585	2.9651	1.527
Blue band	Coefficient	0.0099	0.0055	-0.0007
	p-value	0.0372	0.3739	0.868
	Standard Error	0.0047	0.0062	0.0041
Infrared Band	Coefficient	-0.0087	-0.006	-0.0008
	p-value	0.0001	0.0187	0.6815
	Standard Error	0.0022	0.0025	0.0019
NDVI	Coefficient	-5.1164	-6.8724	-8.9754
	p-value	0.0174	0.0042	0
	Standard Error	2.1378	2.3808	1.8563
IR/R	Coefficient	0.8918	1.004	0.8289
	p-value	0.0113	0.0043	0.0068
	Standard Error	0.3496	0.3486	0.3035
Lambda	Coefficient		0.9364	
	p-value		0	
	Standard Error		0.0344	
AICC		963.03	894.9011	900.4215
Moran's I (residuals)		0.1741		
p-value of Moran's I		0.3814		
p-value (Lagrange)		0		
Likelihood *p*-value			0	0

Figure 2 illustrates different ways of analyzing residuals, including a residuals histogram and graphs of the residuals versus the neighborhood number, predicted values, and the weight of residuals. The residuals histogram has a normal distribution which means that the residuals are spatially independent. The analysis of the residuals versus the neighborhood number, predicted values and

the weight of residuals show that there is no clear trend for any residual which confirms that the residuals are spatially independent.

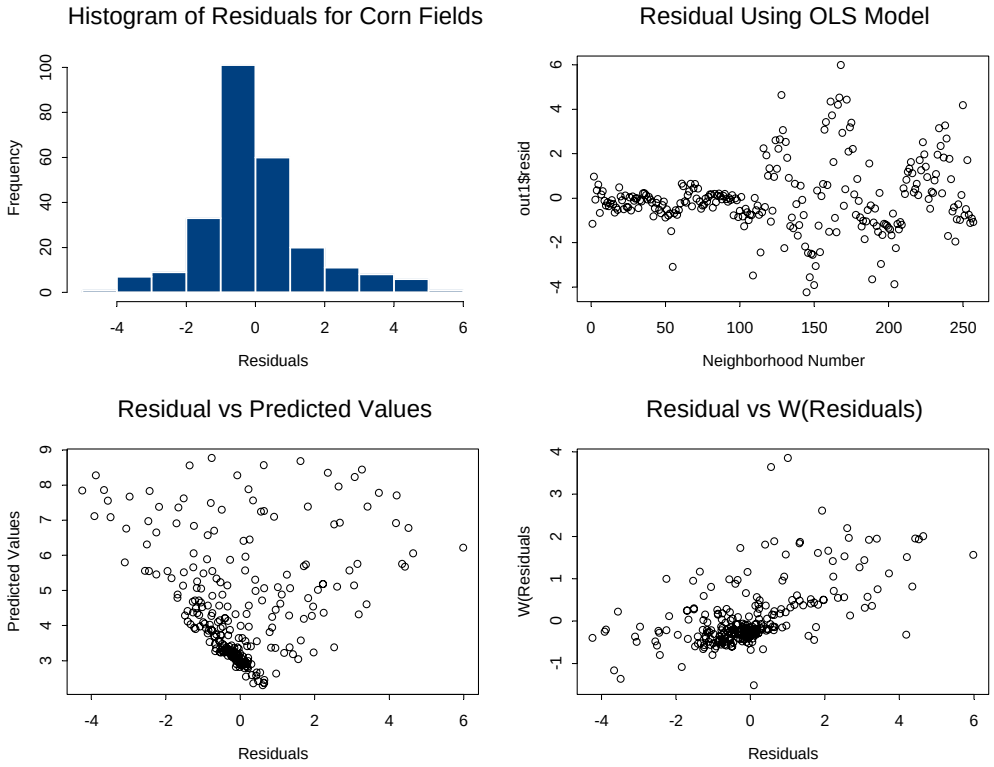

Figure 2. Histogram of residuals and residuals versus neighborhood number, predicted values of soil salinity, and weight of residuals for the OLS when using the blue, infrared, NDVI, and IR/R.

A second set of band combinations was evaluated and the results are shown in Table 2. For this set of band combinations the results show that the SAR model was the best model. The SLAG model was rejected because the p-value of the infrared band was larger than 0.05. The OLS model had a larger AICC than the SAR model, causing the OLS model to be rejected. The equation to predict soil salinity based on the results of the SAR model is:

SAR Predicted soil salinity = 9.6914 – 0.0047 * infrared band – 8.3907 * NDVI + 0.8743 * IR/R.

Table 2. The output variable results of OLS, SAR, and SLAG models using infrared, NDVI, and IR/R.

Variable		OLS	SAR	SLAG
	R^2	0.5157	0.2469	0.2413
	Residual Standard Error	1.5702	1.3295	1.3521
Intercept	Coefficient	11.7136	9.6914	3.1976
	p-value	0	0	0.0001
	Standard Error	0.9092	1.8635	0.7829
Infrared Band	Coefficient	-0.0052	-0.0047	-0.001
	p-value	0.0006	0.024	0.4136
	Standard Error	0.0015	0.0021	0.0013
NDVI	Coefficient	-7.6721	-8.3907	-8.7948
	p-value	0	0	0
	Standard Error	1.767	1.6657	1.5215
IR/R	Coefficient	0.4692	0.8743	0.8566
	p-value	0.1037	0.0063	0
	Standard Error	0.2873	0.3172	1.5215
Lambda	Coefficient		0.9354	
	p-value		0	
	Standard Error		0.0348	
AICC		965.3819	893.6044	898.3511
Moran's I (residuals)		0.1837		
p-value of Moran's I		0.3713		
p-value (Lagrange)		0		
Likelihood *p*-value			0	0

The histogram of residuals shown in Figure 3 has a distribution which is very close to normal, meaning that there is no correlation among the residuals and the residuals are spatially independent. The other three parts of the figure also confirm that there is no correlation among the residuals and that they are spatially independent.

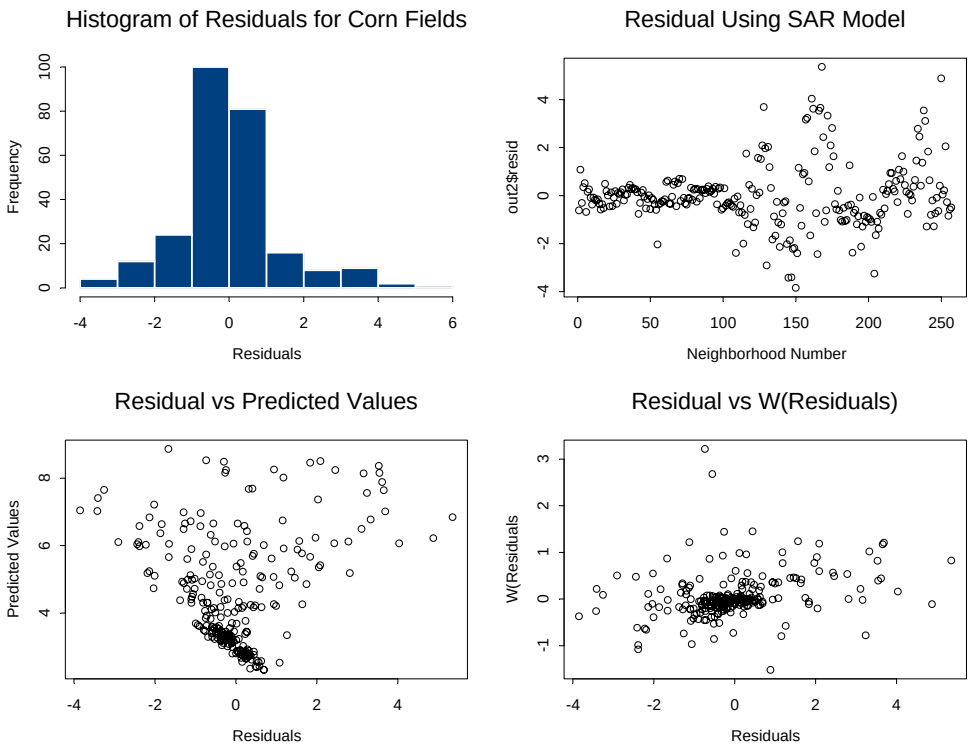

Figure 3. Histogram of residuals and residuals versus neighborhood number, predicted values of soil salinity, and weight of residuals when using the SAR model for infrared, NDVI, and IR/R.

As mentioned earlier, a second approach to detecting soil salinity that we have been testing is to assume that the crop condition is the main indicator of the presence and severity of saline soils. For this approach we selected a field with significant spatial variability in soil salinity (varying from less than 1 dS/m, which causes no crop loss, to over 7.5 dS/m, which inflicts severe corn crop loss) to be our calibration field. A field which fits this criterion is shown in Figure 4. The salinity of the field was determined using georeferenced EM-38 readings. This calibration field allowed us to separate as many salinity classes as possible. Nine different salinity levels were separated from the calibration field. To separate these levels, we spatially linked the satellite image with the soil salinity map derived from field readings. Using a combination of 3 bands (blue, green and near IR) in the satellite image, we selected several pixels that specifically corresponded to a soil salinity level. Reflectance values ranged from 200- 800, with high salinity points clustered around the 700 pixel value, moderate salinity points around the 400-500 pixel value and low salinity points around the 200 pixel value. The classified image was re-coded based on the soil salinity map obtained previously using the EM-38. This re-coding was accomplished by spatially matching each class with the soil salinity values in the same area. This process yielded three classes that represent the severity of soil salinity. The classes were low (0-3.8 dS/m), moderate (3.8-5.8 dS/m) and high (>5.8 dS/m).

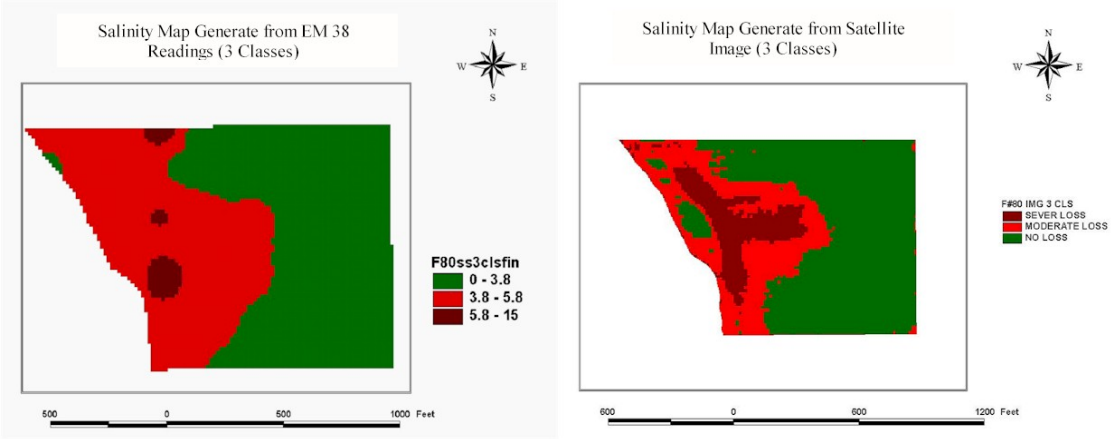

Figure 4. Soil salinity map generated from field data vs. map generated from satellite image.

To examine the accuracy of the satellite generated map, a comparison was done between the ground data map and the re-coded satellite image. The histograms in Figure 5 show this comparison. Fifty five percent of the field-data generated map had soil salinity levels of less than 3.8 dS/m. In the satellite map, 62% of the field registered no loss, indicating salinity levels of less than 3.8 dS/m. Areas where soil salinity levels ranged from 3.8 to 5.8 are considered moderate loss areas and covered 42% of the field in the map generated by the field data. In the satellite image, moderate loss areas comprised 25% of the field area. The highest crop loss falls within areas that have soil salinity of over 5.8 dS/m. These areas encompassed 3% of the field in the field-data generated map. In the satellite image 13% of the field is shown to have severe loss.

To validate this approach, the soil salinity was mapped using an EM-38 in another corn field that falls within the calibrated image. In this validation field, 64 EM-38 soil salinity measurements were taken. A map was generated that shows the severity of the soil salinity in the validation field expressed in terms of low (0-3.8 dS/m), moderate (3.8-5.8 dS/m) and high (>5.8 dS/m) levels.

Table 3 compares the soil salinity map generated from the satellite image with the soil salinity map generated from the EM-38 measurements for the validation field. The comparison shows there was less error when mapping the low salinity areas, which was expected because of the uniformity of the crop in the low salinity areas. No errors were generated when mapping the high salinity zones.

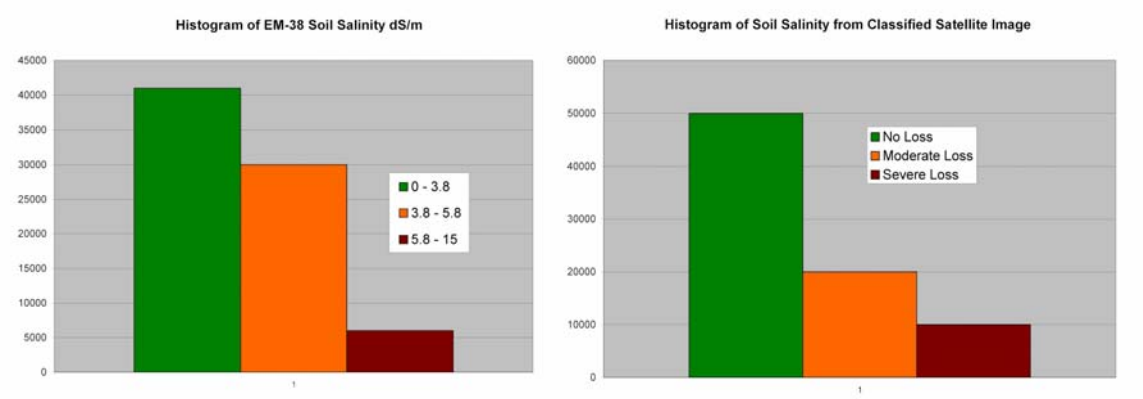

Figure 3. Histogram developed from the maps generated from the EM-38 and the satellite image.

Table 3. Percentage comparisons of salinity levels shown in the two maps.

Class	Ground Data (EM-38)	From Satellite Image
Low salinity	72.53 %	66.17 %
Moderate	22.05 %	21.53 %
High salinity	5.42 %	12.29 %

The over estimation of the high salinity area was because of the existence of a road on the west edge of the field which was classified as a high salinity area because it has no vegetation. Such errors could be eliminated by masking roads and canals as well as bare soil areas (such as barns or feedlots) in the classified image.

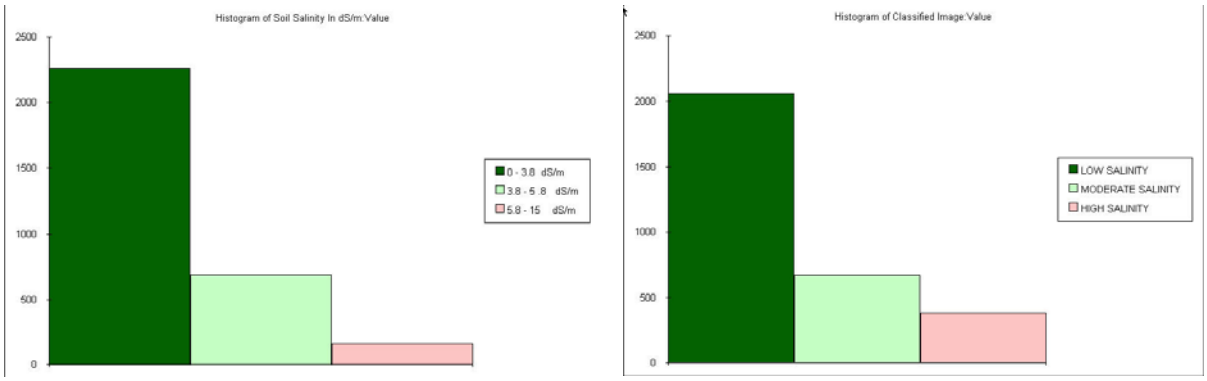

Figure 4. Histogram comparison of the salinity map generated from field data vs. the satellite image map.

SUMMARY AND CONCLUSION

The results presented in this paper show the feasibility of using remote sensing data to estimate soil salinity for corn fields. Compared to the labor, time, and money invested in field work devoted to collecting soil salinity data, the

availability and ease of acquiring satellite imagery is very attractive. The results of our two approaches were:

1) Stepwise regression yields the best combinations of bands to use 90% of the time. The SAR model using the infrared, NDVI, and IR/R combination was evaluated to be the best of all the tested models as it satisfied all the selection criteria and has the smallest AICC value.
2) The approach using crop condition as the main indicator of saline soils has worked very well in our study area. The histogram comparison in Figure 4 shows that the calibrated satellite image matched the data collected with the EM-38 with an overall error of less than 15%.

REFERENCES

Craig, J. C., Shih, S. F., Boman, B. J., & Carter, G. A. (1998). Detection of salinity stress in citrus trees using narrow-band multispectral imaging. *ASAE paper no. 983076. ASAE Annual International Meeting, Orlando, FL, USA,* 12–16 July 1998.

Dwivedi, R.S., and Rao, B.R.M., (1992). "The selection of the best possible Landsat TM band combination for delineating salt-affected soils." *International Journal of Remote Sensing,* 13, 2051–2058.

Ghabour, T.K. and Daels, L. 1993. "Mapping and monitoring of soil salinity of ISSN." *Egyptian Journal of Soil Science* 33: (4)355-370.

Hick, P.T., and Russell, W.G.R. (1990). "Some spectral considerations for remote sensing of soil salinity." *Australian Journal of Soil Research,* 28, 417–431.

Hillel, D. (2000). "Salinity management for sustainable irrigation: integrating science, environment, and economics." *The World Bank:* Washington D.C.

Metternicht, G.I. and Zinck, J.A. (1997). "Spatial discrimination of salt- and sodium-affected soil surfaces." *International Journal of Remote Sensing*, 18, 2571–2586.

Postel, S. (1999). *Pillar of Sand: Can the Irrigation Miracle Last?* W.W. Norton and Co., New York, NY.

Robbins, C.W., and Wiegand, C.L. (1990). "Field and laboratory measurements." *Agricultural Salinity Assessment and Management,* American Society of Civil Engineers, New York.

Szabolcs, I. (1989). *Salt-Affected Soils*. CRC Press, Boca Raton, FL.

Wiegand, C.L., Rhoades, J.D., Escobar, D.E., and Everitt, J.H. (1994). "Photographic and videographic observations for determining and mapping the response of cotton to soil salinity." *Remote Sensing of Environment*, 49, 212-223.